The Arp1/11 minifilament of dynactin primes the endosomal Arp2/3 complex

Artem I. Fokin, Violaine David, Ksenia Oguievetskaia, Emmanuel Derivery, Caroline E. Stone, Luyan Cao, Nathalie Rocques, Nicolas Molinie, Véronique Henriot, Magali Aumont-Nicaise, et al.

BIOCHEMISTRY

The Arp1/11 minifilament of dynactin primes the endosomal Arp2/3 complex

Artem I. Fokin[1]*, Violaine David[2*†], Ksenia Oguievetskaia[1], Emmanuel Derivery[3], Caroline E. Stone[3], Luyan Cao[4], Nathalie Rocques[1], Nicolas Molinie[1], Véronique Henriot[1], Magali Aumont-Nicaise[2], Maria-Victoria Hinckelmann[5], Frédéric Saudou[5], Christophe Le Clainche[2], Andrew P. Carter[3], Guillaume Romet-Lemonne[4], Alexis M. Gautreau[1,6‡]

Dendritic actin networks develop from a first actin filament through branching by the Arp2/3 complex. At the surface of endosomes, the WASH complex activates the Arp2/3 complex and interacts with the capping protein for unclear reasons. Here, we show that the WASH complex interacts with dynactin and uncaps it through its FAM21 subunit. In vitro, the uncapped Arp1/11 minifilament elongates an actin filament, which then primes the WASH-induced Arp2/3 branching reaction. In dynactin-depleted cells or in cells where the WASH complex is reconstituted with a FAM21 mutant that cannot uncap dynactin, formation of branched actin at the endosomal surface is impaired. Our results reveal the importance of the WASH complex in coordinating two complexes containing actin-related proteins.

INTRODUCTION

Dendritic actin networks nucleated by the actin-related protein 2 (Arp2)– and Arp3-containing complex exert pushing forces onto membranes (*1*). The WASH (Wiskott–Aldrich syndrome protein and SCAR homologue) complex activates the Arp2/3 complex at the surface of endosomes and thereby promotes scission of transport intermediates (*2*, *3*). The WASH complex is associated with capping protein (CP) (*2*, *4*). CP is a freely diffusing heterodimer that interacts with the barbed end of actin filaments with high affinity and blocks their elongation (*5*). The FAM21 subunit of the WASH complex displays a conserved CP-interacting motif (CPI) in its extended tail (*6*). CPI motifs directly bind to CP and reduce its affinity for actin filaments through a conformational change (*6*, *7*). The interaction with CPI-containing proteins is thought to bring CP to subcellular locations, where its activity is needed (*8*). Along this model, the WASH complex might thus recruit CP to restrict the growth of endosomal dendritic actin networks, which are small, typically below the diffraction limit of optical microscopy (*9*).

Dynactin, the major activator of the microtubule motor dynein, is a multiprotein complex that contains CP (*10*). Unexpectedly for a microtubule-oriented machinery, dynactin is organized around a minifilament containing one molecule of Arp11, one molecule of β-actin, and eight molecules of Arp1 from the pointed to the barbed end (*11*). The barbed end composed of Arp1 is capped by CP. The WASH complex and dynactin might be in proximity, because the WASH complex is recruited at the endosomal surface through the interaction of FAM21 with the retromer (*12*–*14*) and that dynactin interacts with SNX-BAR sorting nexins, with which the retromer functions (*15*, *16*).

[1]Laboratoire de Biologie Structurale de la Cellule, CNRS, Ecole Polytechnique, IP Paris, Palaiseau, France. [2]Université Paris-Saclay, CEA, CNRS, Institute for Integrative Biology of the Cell (I2BC), Gif-sur-Yvette, France. [3]MRC Laboratory of Molecular Biology, Cambridge, UK. [4]Université de Paris, CNRS, Institut Jacques Monod, Paris, France. [5]Univ. Grenoble Alpes, Inserm, U1216, CHU Grenoble Alpes, Grenoble Institut des Neurosciences, Grenoble, France. [6]School of Biological and Medical Physics, Moscow Institute of Physics and Technology, Dolgoprudny, Russian Federation.
*These authors contributed equally to this work.
†The work of V.D. was initiated and developed in the research team of A.M.G., when the team was still in Gif-sur-Yvette.
‡Corresponding author. Email: alexis.gautreau@polytechnique.edu

RESULTS

Uncapping dynactin

To examine the possibility that dynactin interacts with the WASH complex, we used a transgenic mouse that expresses the dynactin subunit DCTN2 fused to green fluorescent protein (GFP) in the brain (*17*). GFP immunoprecipitates from brain extract contained the WASH complex, suggesting that the two complexes interact, directly or indirectly (Fig. 1A). To inactivate the CPI motif of FAM21, we introduced three point mutations in the residues conserved in all CPI-containing proteins (*6*). The mutated CPI, CPI*, consists of L1024A, R1031A, and P1040A. Compared to wild-type (WT) CPI, CPI* had a 400-fold decreased affinity for CP (Fig. 1B and fig. S1). The three mutations were introduced into full-length FAM21, and stable MCF10A cell lines expressing WT or mutant FAM21 were isolated. FAM21 CPI* did not affect the proper localization of the WASH complex at the surface of endosomes (fig. S2). The CPI* mutations of FAM21 did not affect the integration of FAM21 into the WASH complex, nor the interaction of FAM21 with its partners, FKBP15 and CCDC22 (*12*), but reduced the interaction of FAM21 with CP to undetectable levels (Fig. 1C and fig. S2).

FAM21 CPI and CPI* had no activity on the polymerization of actin, but, as anticipated, CPI, but not CPI*, was able to release the inhibition of filament elongation because of CP, i.e., to "uncap" actin filaments (fig. S3). We reasoned that if CPI was able to uncap dynactin, actin elongation could ensue from the barbed end of the Arp1/11 minifilament. Dynactin induced actin polymerization in the presence of CPI, but not in the presence of CPI* (Fig. 1, D and E, and Table 1). Profilin was added in this assay to suppress spontaneous actin nucleation (*18*). We next sought to visualize filament growth using total internal reflection fluorescence (TIRF) microscopy. To this end, we purified GFP-labeled dynactin through tandem affinity purification and anchored it via the GFP-binding protein (GBP) to a passivated coverslip. When dynactin was anchored, infusion of profilin-actin initiated the elongation of a few actin filaments (Fig. 1F). This basal activity of dynactin was suppressed by the addition of purified CP, suggesting that some dynactin complexes immunoprecipitated from cells were already uncapped. The number of elongating actin filaments was, however, significantly

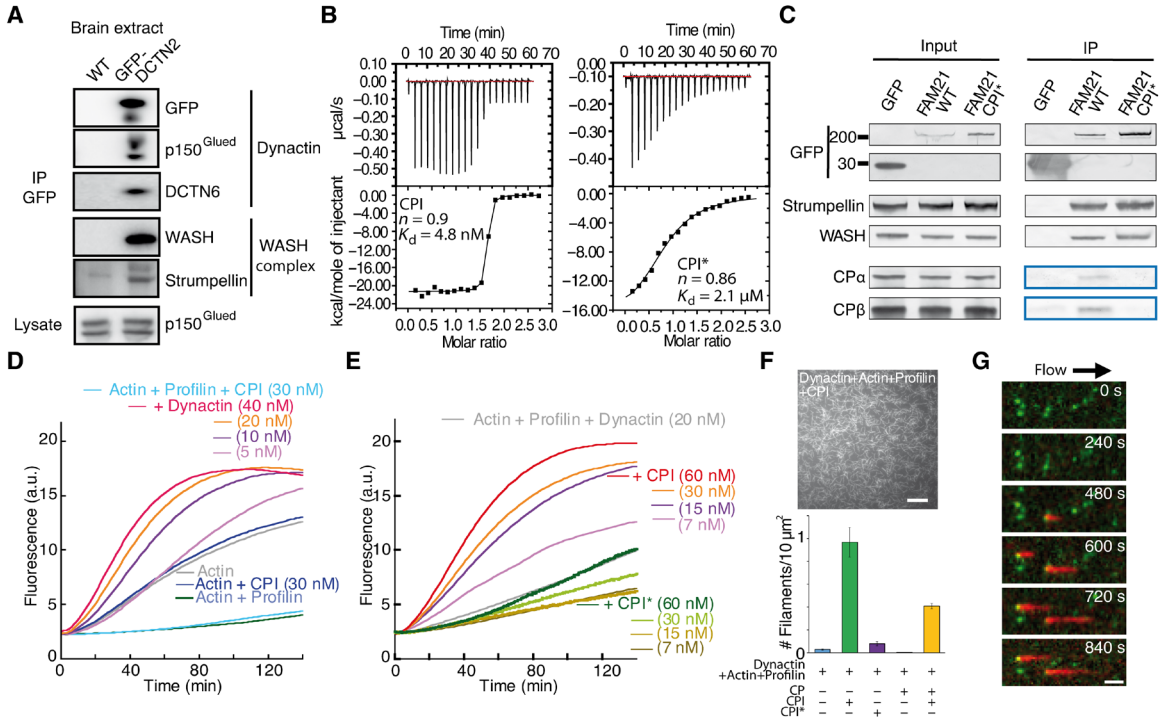

Fig. 1. The CPI motif of FAM21 induces actin elongation from dynactin. (**A**) The WASH complex coprecipitates with GFP-tagged dynactin (GFP-DCTN2) from the brain of a transgenic mouse. (**B**) Isothermal calorimetry of the interaction between CP and WT CPI or CPI*, a variant containing three point mutations. Curve fits indicate the stoichiometry of interaction (*n*) and K_d (dissociation constant). (**C**) Stable expression of GFP-FAM21 CPI* in MCF10A cells reconstitutes a WASH complex that does not recruit CP. (**D** and **E**) Pyrene-actin polymerization assays. Conditions: 2.0 µM actin (5% labeled), 8 µM profilin, native dynactin, CPI, or CPI*. a.u., arbitrary units. (**F**) TIRF imaging of filaments elongated from surface-anchored dynactin in the presence of CPI. Observation 10 min after having introduced 1 µM labeled actin, 8.2 µM profilin, 0 or 2 µM CP, and 0 or 2.7 µM CPI in F-buffer. Scale bar, 20 µm. (**G**) Time-lapse images of actin filaments growing under flow from GFP-DCTN3–labeled dynactin (green). Conditions: 1 µM actin (15% labeled, red), 1 µM profilin, 50 nM CPI. Scale bar, 3 µm.

Table 1. Concentration of barbed ends in pyrene-actin assays.

Fig. 1D	**Actin (2 µM)**			**Actin (2 µM) + Profilin (8 µM) + CPI (30 nM)**				
	–	+ CPI (30 nM)	+ Profilin (8 µM)	–	+ Dynactin (5 nM)	+ Dynactin (10 nM)	+ Dynactin (20 nM)	+ Dynactin (40 nM)
Barbed ends at 30 min (pM)	15.6	18.7	2.6	2.4	25.6	56.8	81.1	106.4

Fig. 1E	**Actin (2 µM) + Profilin (8 µM) + Dynactin (20 nM)**							
	+ CPI (7 nM)	+ CPI* (7 nM)	+ CPI (15 nM)	+ CPI* (15 nM)	+ CPI (30 nM)	+ CPI* (30 nM)	+ CPI (60 nM)	+ CPI* (60 nM)
Barbed ends at 30 min (pM)	24.3	3	40.5	5.3	51.5	7.47	74.4	6

Fig. 3C	**Actin (2 µM) + Profilin (3 µm) + Dynactin (10 nM)**			**Actin (2µM) + Profilin (3 µM) + Arp2/3 (20 nM) + VCA (70 nM)**		
	–	+ CPI	+ CPI later	–	+ Dynactin (10 nM)	+ Dynactin (10 nM) + CPI (50 nM)
Barbed ends at 15 min (pM)	0.43	26.1	12.5	53.7	64.6	154.2

enhanced by CPI, but not by CPI*. Similar results were obtained with dynactin purified and anchored via GFP-Arp1 or via GFP-DCTN3 (Fig. 1F and fig. S4A). The growth rate of elongating filaments unambiguously indicated that growing occurs through the barbed end (movie S1 and fig. S4B). We then used microfluidics and a sparse density of anchored GFP-labeled dynactin to monitor filament elongation. Upon addition of CPI, the vast majority of filaments elongated from a green dot corresponding to a single anchored dynactin complex (Fig. 1G and fig. S4, C and D). The rare occurrences where filaments did not elongate from a green dot are likely to correspond to elongation from a bleached dynactin complex, because filament fluctuations in the flow systematically indicated that filaments were specifically attached through an end (movie S2). The simplest hypothesis that can account for all these observations is that dynactin becomes uncapped by CPI.

To directly examine dynactin uncapping, we took advantage of our dually tagged versions of dynactin (His-mCherry-CPα with either Flag-GFP-Arp1 or Flag-GFP-DCTN3). Anchored dynactin displayed high levels of colocalization of green and red spots, which were reduced upon incubation with CPI, but not CPI* (Fig. 2A). The single mCherry fluorophore was more prone to bleaching than the GFP (up to eight copies for Arp1, up to two copies for DCTN3). This suggests that CPI dissociates CP from the rest of dynactin. To unambiguously establish this point, we analyzed native dynactin by gel filtration. Upon incubation with CPI, but not with CPI*, part of CP migrated in low–molecular weight fractions and was thus no longer associated with the dynactin peak (Fig. 2B; fig. S5 for full gels). Dynactin fractions incubated with CPI or not were negatively stained and imaged by electron microscopy (EM). From the CPI-treated sample, most single particles fell into two three-dimensional (3D) classes that appeared to have lost density at the end of the rod-shaped structure (Fig. 2C and fig. S6). Docking a structural model of native dynactin into the density map shows that dynactin treated with CPI no longer accommodates CP at the barbed end of the Arp1/11 minifilament (Fig. 2D). Together, these experiments demonstrate that dynactin is uncapped when treated with CPI and that the uncapped dynactin is a stable complex.

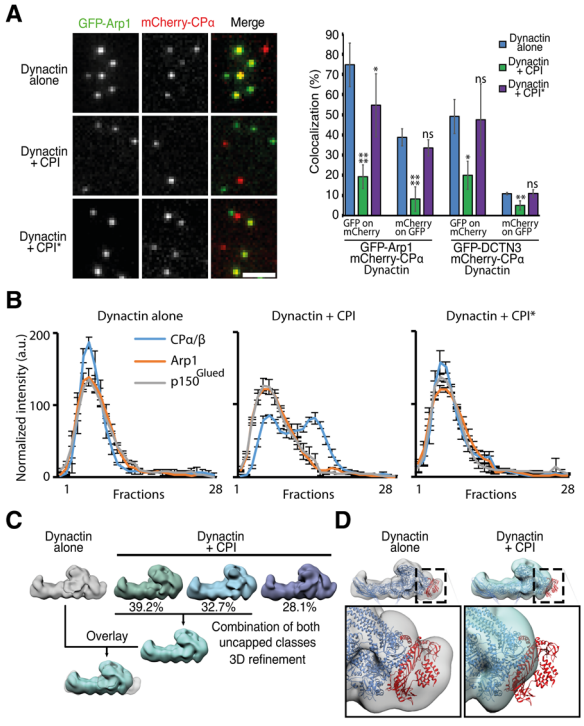

Fig. 2. FAM21 CPI removes CP from the Arp1/11 minifilament of dynactin. (**A**) Single dynactin complexes containing GFP-Arp1 and mCherry-CPα were observed by TIRF microscopy. Quantification of the colocalization of green and red spots. Conditions: 40 nM dynactin preincubated with 2.7 μM CPI or CPI* for 1 min was diluted 10-fold and then adsorbed on the coverslip surface. Scale bar, 5 μm. (**B**) Distribution of dynactin subunits in gel filtration in the presence of CPI or CPI*. (**C**) Elution fractions containing dynactin were negatively stained and observed by EM. Two major classes of 3D reconstructions obtained in the presence of CPI appear to lack a specific density. (**D**) The previously obtained cryo-EM model of dynactin was fit into the negative-stain EM densities. The two CP subunits are in red; other dynactin subunits are in blue. ns, not significant.

Arp2/3 priming

The actin filament elongated from dynactin might be useful to initiate an actin branching reaction. The activated Arp2/3 complex nucleates a filament when it lands on a preexisting filament (*19*). Because the actin filament is both a substrate and a product of the reaction, the generation of dendritic actin networks is an autocatalytic process that requires a first primer filament to get started (*20*). We verified that uncapped dynactin can provide such a primer filament in a single-filament TIRF assay. To this end, dynactin was first uncapped by CPI in the presence of red actin and profilin. The resulting filaments were then mixed with the Arp2/3 complex, green actin, and the Arp2/3-activating VCA motif of WASH. Numerous green filaments branched out from red actin filaments elongated from dynactin (Fig. 3A and movie S3). The density of actin branches was similar on filaments elongated from dynactin (0.31 ± 0.11 branches per micrometer, n = 15) and on spontaneously nucleated actin filaments (0.28 ± 0.12 branches per micrometer, n = 19). At later time points, numerous dendritic actin structures had developed, most of them from a single red actin filament (Fig. 3B). In bulk actin polymerization assays, the effect of dynactin uncapping was discernible, but not as notable, likely because Arp2/3-mediated polymerization can be initiated from the first spontaneously nucleated actin filament that had escaped the suppressive effect of profilin (Fig. 3C and Table 1). Uncapped dynactin is thus competent to initiate the formation of dendritic actin structures.

The WASH complex activates the Arp2/3 complex at the surface of endosomes (*2*, *3*). To examine whether dynactin was present in endosomal dendritic actin structures, we derived a triple transgenic MCF10A cell line stably expressing GFP-tagged ARPC5 (Arp2/3), mCherry-tagged DCTN6 (dynactin), and iRFP670-tagged WASH. In this cell line, fusion proteins are not present in excess and incorporate into their respective complexes as shown by sucrose gradient and immunoprecipitation (fig. S7, A and C). We chose to tag DCTN6, because this peripheral subunit is important for the association of dynactin with membranes (*21*). Using fast live-cell imaging, DCTN6-tagged dynactin exhibited the expected behavior of microtubule + end tracking (movie S4). Some endosomal compartments transiently appeared simultaneously positive for WASH, Arp2/3, and dynactin (Fig. 3D and fig. S7, D and E). WASH and Arp2/3 spots were more often colocalized than WASH and dynactin spots (59 ± 2% versus 6.2 ± 0.9%, mean ± SEM, 1587 WASH spots in 28 cells). Kymograph analyses indicated that this association cannot be decomposed into a stereotypical sequence of events. Unlike clathrin-coated pits, where branched actin polymerization is precisely coordinated with membrane

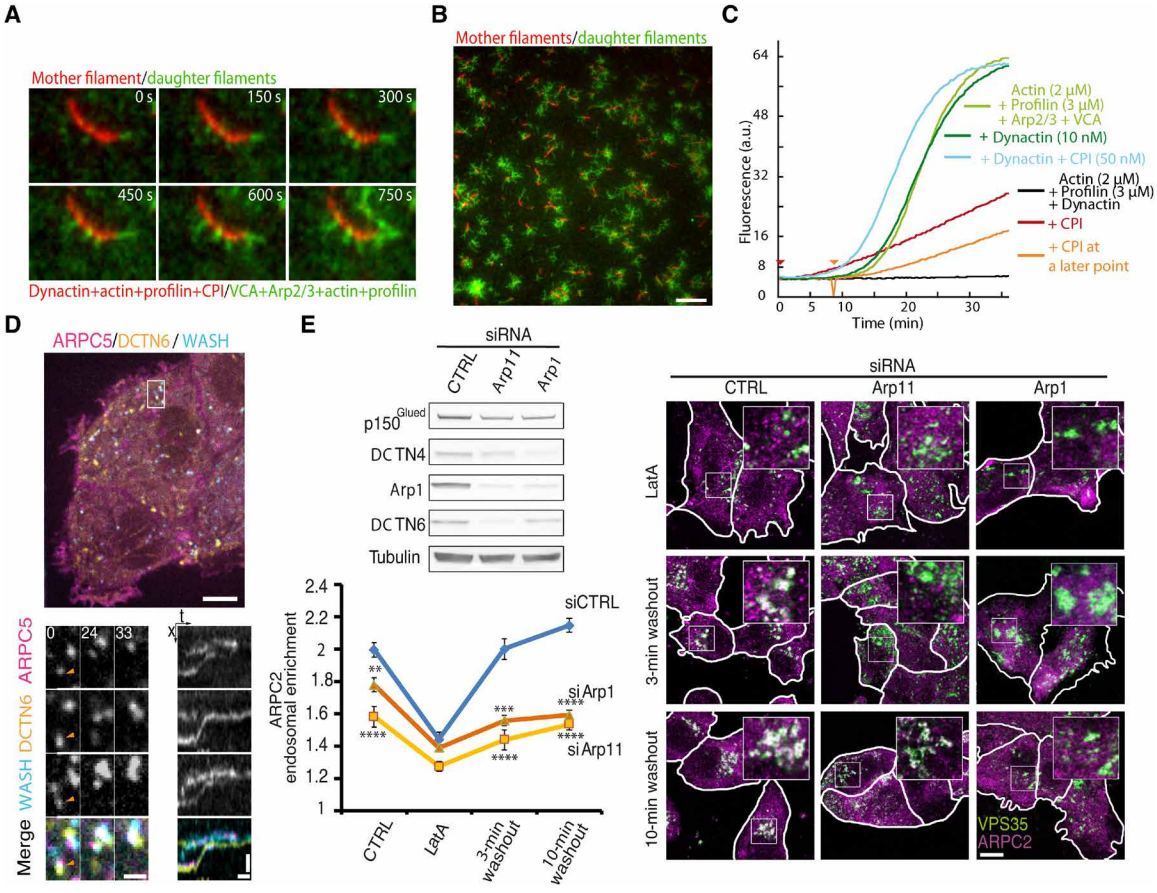

Fig. 3. Dynactin primes endosomal branched actin structures. (**A**) The filament elongated from dynactin provides a substrate for actin branches (TIRF microscopy). Dynactin (2 nM) was preincubated for 12 min in F-buffer with 270 nM CPI, 1 μM profilin, and 0.8 μM Alexa 568–actin (red, 15% labeled). The reaction was then diluted 20-fold in a solution containing 60 nM WASH VCA 60 nM Arp2/3, 0.4 μM profilin, and 0.4 μM Alexa 488–actin (green, 15% labeled) in F-buffer supplemented with 0.13% methylcellulose. Scale bar, 2 μm. (**B**) Whole field of view from the experiment in (A) after 1500 s. Scale bar, 10 μm. (**C**) Pyrene-actin polymerization assay. Conditions: Actin (2 μM, 5% pyrene), profilin (3 μM), native dynactin (10 nM), CPI (50 nM), Arp2/3 (20 nM), and VCA (70 nM). Addition of the CPI fragment is indicated by arrowheads. (**D**) Live spinning disk confocal microscopy of an MCF10A cell line stably expressing GFP-ARPC5 (Arp2/3), mCherry-DCTN6 (dynactin), and iRFP-WASH. Single confocal plane. Scale bar, 6 μm. Middle: Zoomed still images extracted from the video (white box), elapsed time in seconds; scale bar, 1.2 μm. Right: Kymograph; scale bars, vertical 1.2 μm, horizontal 12 s. (**E**) MCF10A cells were depleted of dynactin through siRNAs targeting Arp1 or Arp11. Endosomal branched actin structures were estimated by the overlap of ARPC2 (Arp2/3) with VPS35 (retromer) upon latrunculin A (LatA) washout. Scale bar, 10 μm.

scission (*22*), dendritic actin networks participate to several functions at the surface of endosomes in addition to membrane scission, such as tubule elongation, organization of membrane microdomains, and prevention of endosome clumping (*9*, *23*, *24*).

Our in vitro reconstitution indicated that dynactin should be required for the formation of branched actin in the physiological presence of profilin. Thus, we depleted dynactin by targeting the minifilament forming subunits Arp1 and Arp11 and analyzed endosomal dendritic actin structures. At steady state, dendritic actin structures associated with the retromer were decreased (Fig. 3E). This effect was enhanced in a dynamic regrowth assay after washout of the actin depolymerizing drug latrunculin A. Although endosomal WASH complexes could still, in principle, bind to the Arp2/3 complex, this result illustrates how formation of dendritic actin networks containing Arp2/3 at each branch is impaired upon dynactin depletion. To our knowledge, this is the first example of actin polymerization that requires dynactin. Because the depletion of dynactin affects numerous cellular functions, we complemented this result by the phenotypic analysis of cells expressing FAM21 CPI*.

Uncapping by WASH

When we knocked down endogenous FAM21 using small interfering RNAs (siRNAs) targeting the 3′ untranslated region (3′UTR) of FAM21, expression of FAM21 WT or CPI* restored normal levels of FAM21 and of WASH to the surface of endosomes (fig. S8). In sharp contrast, however, only FAM21 WT, and not FAM21 CPI*, was able to restore dendritic actin networks at the surface of endosomes (Fig. 4A). This experiment indicates that the interaction of the WASH complex with CP does not restrict the growth of endosomal branched actin. Rather, the ability of the WASH complex to uncap dynactin is critical to generate dendritic actin networks at the surface of endosomes. We next examined the cell functions ascribed to the WASH complex in this system, where WASH complexes are present, but deficient in polymerizing branched actin. Using live imaging of cells loaded with fluorescent transferrin, we observed that knockdown of FAM21 led to an increase in endosome size and tubulation (Fig. 4B), as previously described (*2*, *3*, *9*). These defects indicate an impaired scission of the transport intermediates that sort endosomal cargoes (*24*). We found that FAM21 WT, but not

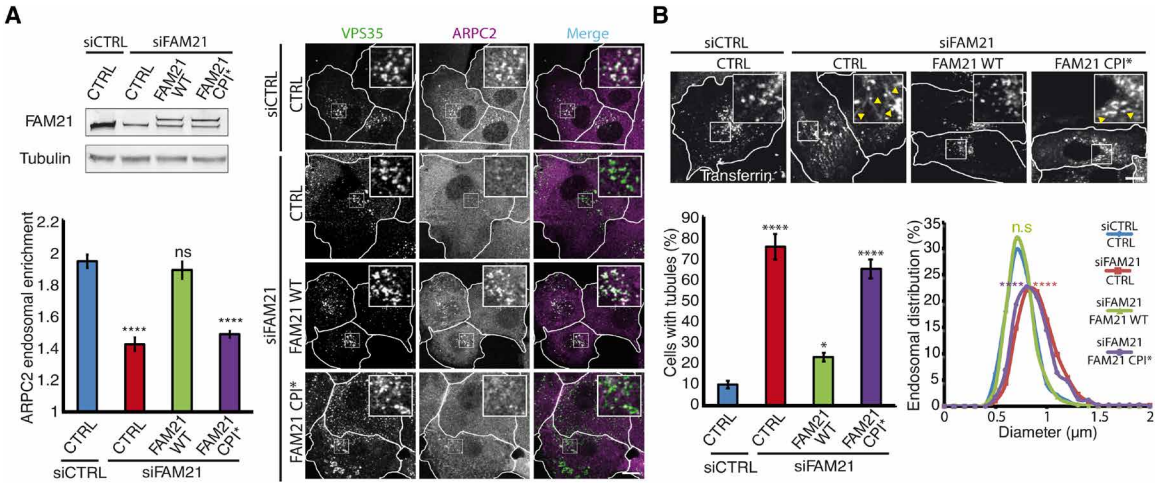

Fig. 4. Deficient uncapping alters endosomal structures. (**A**) Endogenous FAM21 was depleted from MCF10A control cells or stable MCF10A lines expressing GFP-FAM21 WT or CPI* using siRNAs. Endosomal branched actin structures were estimated by the overlap of ARPC2 (Arp2/3) with VPS35 (retromer). Scale bar, 10 μm. (**B**) Endosomes were loaded at steady state with fluorescent transferrin. Endosomal size and the presence of tubules (arrowheads) were estimated from live-cell confocal imaging.

CPI*, was able to rescue the morphological defects induced by FAM21 knockdown.

We studied the recycling of two well-established WASH-dependent cargoes, integrins (*25*, *26*) and the GLUT1 glucose transporter (*27*, *28*). Levels of β1 integrins were down-regulated in FAM21-depleted cells (Fig. 5, A and B), because of their deficient recycling to the plasma membrane following internalization in the absence of functional WASH complex (Fig. 5, C and D). FAM21-depleted cells were able to protrude efficiently, but several protrusions often stretched cells in different directions, resulting in frequent shape changes, captured by aspect ratio volatility (Fig. 5E, movie S5, and fig. S9A). Overall, FAM21-depleted cells explored a larger surface area than controls (Fig. 5E and fig. S9, B and C), as indicated by their mean square displacement. FAM21 WT, but not CPI*, rescued β1-integrin recycling defects and aberrant cell migration. Recycling of GLUT1 from endosomes to the plasma membrane requires the sorting nexin SNX27 and the WASH complex (*27*). FAM21 knockdown accumulated GLUT1 in SNX27-positive endosomes at the expense of the plasma membrane. FAM21 WT, but not FAM21 CPI*, restored GLUT1 at the plasma membrane (Fig. 5F). The lack of GLUT1 at the plasma membrane translated into a profound defect in the uptake of 2-NitroBenzoxaDeoxyGlucose (2-NBDG), a fluorescent glucose analog (Fig. 5G and fig. S9D).

DISCUSSION

The lack of rescue by FAM21 CPI* in these structural and functional analyses is notable considering that essential endosomal machinery is present in these experiments and that the only defect in the WASH complex reconstituted with FAM21 CPI* is its ability to interact with CP. Together, our in vitro reconstitutions and cell biology experiments support a working model where the WASH complex coordinates two multiprotein complexes containing distinct Arps (fig. S9E and movie S6). The WASH complex is the only stable multiprotein complex that combines CPI and VCA motifs. WASH first uncaps dynactin through the CPI of FAM21. The barbed end elongation from uncapped dynactin then provides a primer actin filament for the Arp2/3 autocatalytic reaction.

We found that the CPI motifs of CARMIL and CIN85 can also induce actin elongation by uncapping dynactin in vitro, indicating that the mechanism of dynactin uncapping is similar to the uncapping of an actin filament (fig. S10). These two proteins, however, which associate with dendritic actin networks at the lamellipodial edge (*29*, *30*) and clathrin-coated pits (*31*, *32*), respectively, do not appear to colocalize with dynactin in the cell (movies S7 and S8). Uncapping dynactin to provide a primer filament to the Arp2/3 branching reaction is critical at the surface of endosomes, but probably not at the cell cortex, which is already rich in actin filaments.

Our newly discovered role of dynactin in regulating actin polymerization complements its well-characterized function in promoting transport along microtubule tracks. Dynactin is organized around a central Arp minifilament, which recruits dynein adaptor proteins along its length (*33*) and that primes the Arp2/3 complex via the elongation of an actin filament from its barbed end. Actin and microtubule cytoskeletons are both involved in controlling shape, motility, and scission of endosomes. Dynactin thus plays a critical role toward both of these cytoskeletal elements at the surface of endosomes.

MATERIALS AND METHODS

Plasmids

All open reading frames (ORFs), or fragments thereof, were flanked by Fse I and Asc I restriction sites for easy shuttling between compatible plasmids. All polymerase chain reaction (PCR)–amplified fragments were sequenced to ensure that no unwanted mutation was introduced. Custom-made plasmids were created using the MXS building block strategy (*34*).

WASH complex

FAM21 (FAM21C, NP_001317003) was amplified from the pCM3.H1p.shFAM21C.HA YFP FAM21C construct provided by D. Billadeau (Mayo Clinic, Rochester, MN, USA). FAM21 CPI corresponds to the fragment called U3A (*14*), i.e., the peptide 934–1071 (ETPQ–QWAD). The CPI* mutations L1024A, R1031A, and P1040A were introduced into the CPI fragment or full-length FAM21 by QuikChange site-directed mutagenesis (Agilent). WASH ORF and VCA were previously described (*2*).

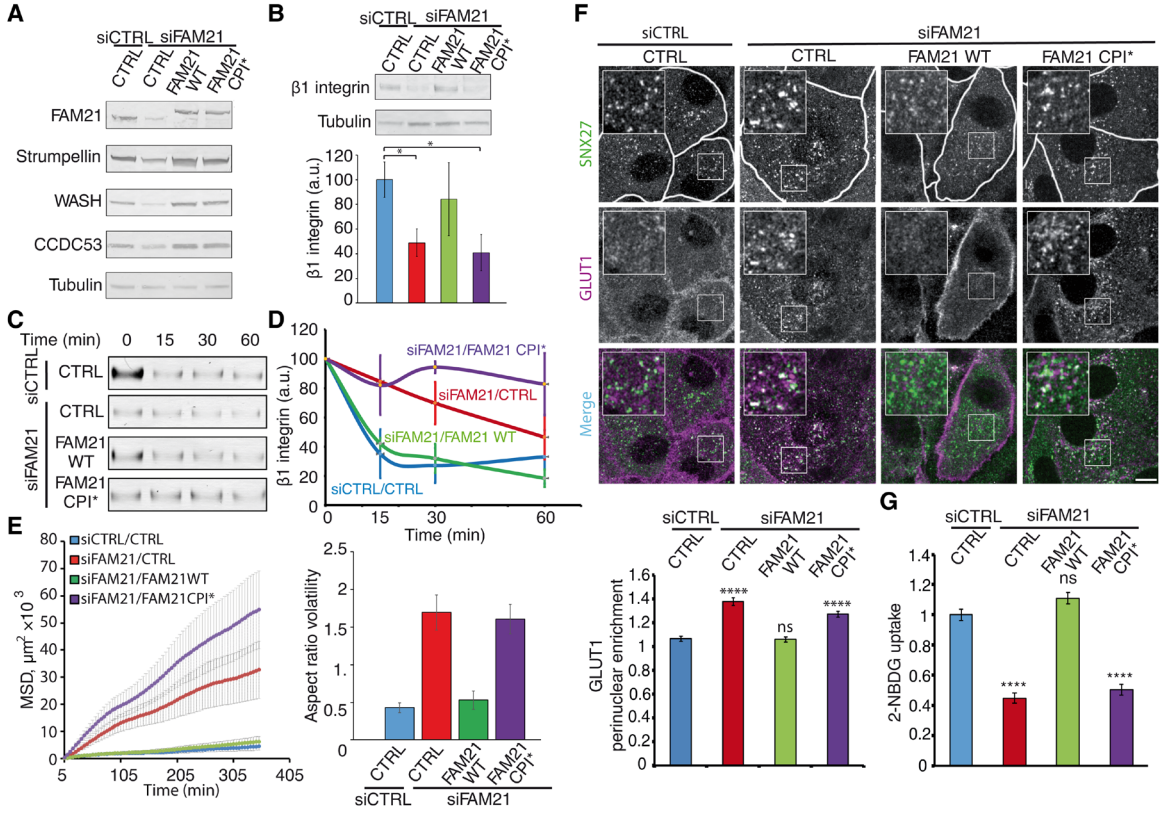

Fig. 5. Uncapping by the WASH complex is required for cargo recycling. (**A**) Endogenous FAM21 was depleted from MCF10A control cells or stable MCF10A lines expressing GFP-FAM21 WT or CPI* using siRNAs. WASH complex subunits were analyzed by Western blots. (**B**) Levels of β1 integrin and quantification by densitometry. (**C**) β1-integrin recycling. Surface proteins that were biotinylated and internalized were allowed to recycle to the plasma membrane for the indicated time, before extracellular exposed biotin was removed. Streptavidin-captured protein was analyzed by β1-integrin Western blots. (**D**) Quantification by densitometry. (**E**) Mean square displacement (MSD) and aspect ratio volatility of single cells. (**F**) The glucose transporter GLUT1 localizes to perinuclear SNX27-positive endosomes and at the plasma membrane. Scale bar, 10 μm. (**G**) Cell uptake of the glucose analog 2-NBDG.

Arp2/3 complex

ARPC5 and ARPC1B were amplified from described plasmids (*35*, *36*).

Dynactin

ORFs encoding human Arp1, DCTN3, and DCTN6 were amplified by PCR from IMAGE clone numbers 3009822, 6454606, and 3925231, respectively. CARMIL1 (also known as LRRC16A) was amplified from IMAGE clone 9021638. CARMIL1 CPI corresponds to the fragment called CBR (*30*), i.e., peptide 964–1078 (EKRS–KSRS).

CIN85 (also known as SH3KBP1) was amplified from IMAGE clone 3906722. CIN85 CPI corresponds to the peptide 426–523 (VGPL–ISLA). CPα, which was amplified by PCR from pRFSDuet encoding the His-tagged α1 and β2 subunits of murine CP, was from P. Lappalainen (University of Helsinki, Finland). GBP was obtained by gene synthesis (*37*).

Plasmids for protein production

CPI peptides from FAM21, CARMIL1, and CIN85 were cloned into pET28b for *Escherichia coli* expression as a His-tag fusion protein. FAM21 CPI and CPI* were also cloned into pGEX CS for *E. coli* expression as a glutathione *S*-transferase (GST) fusion protein. pGEX-WASH VCA was described (*2*). pRFSDuet encoding the His-tagged α1 and β2 subunits of murine CP allows purification of the CP heterodimer. The GBP was cloned into a modified pET28b vector encoding a fusion protein with His tag and the Avitag sequence, which is biotinylated by BirA.

Plasmids for expression in human cells

Rescue plasmids. FAM21 CPI WT and CPI* were cloned into MXS AAVS1L SA2A Puro bGHpA PGK rtTA3 SV40pA TRE EGFP Blue SV40pA AAVS1R and MXS PGK Blasti bGHpA EF1Flag iRFP Blue SV40pA.

Tandem affinity purification. Arp1 and DCTN3 were inserted into pCDNAm FRT Flag-GFP vectors (*2*). CPα was inserted into MXS PGK Puro bGHpA EF1α 6His PC Cherry CapZa SV40pA.

Live-cell imaging experiments required construction of the following:

MXS AAVS1L SA2A Puro bGHpA EF1Flag EGFP ARPC5 SV40pA AAVS1R

MXS PGK Puro bGHpA EF1Flag EGFP CARMIL1 SV40pA
MXS PGK Puro bGHpA EF1Flag EGFP CIN85 SV40pA
MXS PGK Zeo SV40pA EF1Flag mCherry DCTN6 SV40pA
MXS PGK Zeo SV40pA EF1Flag mCherry Arp1 SV40pA
MXS PGK Blasti SV40pA EF1Flag iRFP WASH SV40pA
MXS PGK Blasti SV40pA EF1Flag iRFP ARPC1B SV40pA

Cells and transfections

The immortalized epithelial cell line from human breast, MCF10A, was cultured in Dulbecco's modified Eagle's medium (DMEM)/F12 medium (Gibco) supplemented with 5% horse serum (Sigma-Aldrich), cholera toxin (100 ng/ml; Sigma-Aldrich), epidermal growth factor

(20 ng/ml; Sigma-Aldrich), insulin (0.01 mg/ml; Sigma-Aldrich), hydrocortisone (500 ng/ml; Sigma-Aldrich), and penicillin/streptomycin (100 U/ml; Gibco). These cells were transfected with plasmids using Lipofectamine 3000 (Invitrogen). To obtain homologous recombination at the well-expressed AAVS1 locus, constructs were cotransfected with AAVS1 TALEN constructs (Addgene numbers 59025 and 59026) (*38*). Two days after transfection, the appropriate selective antibiotic is added (1 μg/ml puromycin, 8 μg/ml blasticidin, 100 μg/ml zeocin). Single clones were isolated by cloning rings, expanded, and characterized. To induce GFP-FAM21, 2 days of doxycycline treatment at 2 μg/ml were used. For siRNA-induced depletion of proteins, cells were transfected twice with 20 nM targeting siRNA (Sigma-Aldrich) at day 0 and at day 2 using Lipofectamine RNAiMAX (Invitrogen). Cells were harvested or fixed at day 5. The following siRNAs were used: CTRL, AAUUCUCCGAACGUGUCACGUUU; FAM21 3′UTR, GCAAAUACUAGAACAGCUAGCUU; ARP1 (ACTR1A), GCUUUCUUGAGUCGGAGUGUUUU; ARP11, GCGCGUACUUGCUUUGUAAdTdT (*21*).

A total of 293 FlpIn. TREx cells containing a single FRT site at a well-expressed locus (Invitrogen) were grown in DMEM supplemented with 10% fetal calf serum (Invitrogen), zeocin (50 μg/ml; InvivoGen), and blasticidin (5 μg/ml; InvivoGen). Cells were transfected by calcium phosphate precipitation with pCDNAm plasmids expressing Flag-GFP–tagged dynactin subunits and the Flp recombinase encoding pOG44 (Invitrogen). Pools of stable transfected cells were selected with hygromycin (200 μg/ml; InvivoGen). These stable cells were then transfected with MXS PGK Puro bGHpA EF1Flag mCherry CPα SV40pA and selected with puromycin (1 μg/ml) (InvivoGen). Stable dual clones were isolated and expanded in spinners for a total volume of 6 liters as described (*39*).

Antibodies

For immunofluorescence, the following antibodies were used: GLUT1 rabbit polyclonal antibody (pAb) and SNX27 mouse monoclonal antibody (mAb) from Abcam (ab15310 and ab77799, respectively); VPS35 (B-5) was from Santa Cruz Biotechnology. For Western blots, the following antibodies were used: pAb to strumpellin (C-14) and mAbs to Arp1/ACTR1 (α/β centractin, E-5); polyclonal Arp3 (number 07–272) was from Cell Signaling; p62/DCTN4 (H-4) were from Santa Cruz Biotechnology; ArpC5 mAb (clone 323H3) was from Synaptic Systems; tubulin mAb (clone DM1A) was from Sigma-Aldrich; $p150^{Glued}$/DCTN1 and β1-integrin mAbs were from BD Biosciences (BD610474 and BD610468, respectively); GFP mAbs (13.1 and 7.1 clones) were from Roche; CPα and CPβ mAbs (5B12.3 and 3F2.3, respectively) were from Developmental Studies Hybridoma Bank; rabbit pAb to p27/DCTN6 (16948-1-AP) was from Proteintech; home-made polyclonal rabbit antibody CCDC53 was previously described (*2*, *40*). For both applications, the following antibodies were used: home-made polyclonal rabbit antibodies targeting WASH and FAM21 were previously described (*2*, *40*); ARPC2 rabbit pAb was from Millipore (07-227).

Secondary goat anti-mouse and anti-rabbit antibodies conjugated with Alexa Fluor 488, 555, and 647 used for immunofluorescence were from Life Technologies. Secondary goat anti-mouse and anti-rabbit antibodies conjugated with alkaline phosphatase used for Western blots were from Promega.

Laboratory animals

Adult Thy1:p50-GFP male mice were kept in 12:12-hour light/dark cycle at constant temperature (19° to 22°C), food and water ad libitum. All experimental procedures were performed in an authorized establishment (Institut Curie, Orsay facility license number C91471108, February 2011) in strict accordance with the recommendations of the European Community (86/609/EEC) and the French National Committee (2010/63) for care and use of laboratory animals under the supervision of authorized investigators (permission number 91-448 to S. Humbert). This study was evaluated and approved by the ethics committee, "Comité d'éthique en matière d'expérimentation animale Paris Centre et Sud" (national registration number: #59), presided by P. Bigey.

Immunoprecipitations and Western blots

Each mouse brain was homogenized in the following buffer: 50 mM Hepes (pH 7.7), 100 mM KCl, 1 mM $MgCl_2$, 1% Triton X-100, 320 mM sucrose supplemented with the cOmplete, EDTA free Protease Inhibitor Cocktail (Roche). The homogenate was purified by two subsequent centrifugations at 4°C (10 min at 1000*g* and 40 min at 12,000*g*) to remove nuclei and obtain a crude cytoplasmic fraction used for immunoprecipitation. MCF10A cells expressing GFP-FAM21 were lysed in buffer (50 mM Hepes, 200 mM NaCl, 1 mM $CaCl_2$, 5 mM $MgCl_2$, 5% glycerol, 1% Triton X-100, pH 7.4) supplemented with protease inhibitors. Cell extracts were incubated with 15 μl of GFP-trap beads or RFP-trap beads (Chromotek) for 2 hours at 4°C, washed extensively with lysis buffer, and resuspended in SDS loading buffer. SDS–polyacrylamide gel electrophoresis (SDS-PAGE) was performed using NuPAGE 4 to 12% bis-tris or 3 to 8% tris-acetate gels (Thermo Fisher Scientific). After transfer, nitrocellulose membranes were blocked in 5% milk and incubated with primary and secondary antibodies. For Western blots analyzed by densitometry, the intensity of a rectangle area containing the band of interest with a subtracted background was divided by the intensity of a similar rectangle containing α-tubulin staining of the same blotting membrane. The intensities were normalized to 100% in control conditions and plotted. For the densitometry analysis of dynactin subunits in Fig. 2B, values for each dynactin subunit were normalized by the area under curve.

Sucrose gradient

Nitrogen cavitation (Parr Instrument, 500 psi for 20 min) followed by centrifugation (16,000*g*, 20 min) and ultracentrifugation (150,000*g*, 60 min) was used to prepare cytosolic extracts from cells trypsinized from two 15-cm dishes and resuspended in the XB buffer [20 mM Hepes, 100 mM NaCl, 1 mM $MgCl_2$, 0.1 mM EDTA, 1 mM dithiothreitol (DTT), pH 7.7]. Two hundred microliters of extract was loaded on the 11-ml 5 to 20% sucrose gradient in the XB buffer and subjected to ultracentrifugation for 17 hours at 197,000*g* in the swinging bucket rotor SW41 Ti (Beckman). Fractions (0.5 ml) were collected and concentrated by using trichloroacetic acid precipitation with insulin as a carrier. The samples were washed with acetone, dried, and then resuspended in the 1× LDS loading buffer with 2.5% β-mercaptoethanol (β-ME) for Western blot analysis.

Recombinant protein purification

All recombinant proteins were expressed in the BL21* strain (Invitrogen). The WASH VCA fragment was purified in fusion with GST as described (*2*). After concentration on Amicon Ultra (Millipore), it was dialyzed against buffer [20 mM tris (pH 7.5), 25 mM KCl, 1 mM $MgCl_2$, 150 μM sucrose], flash-frozen in liquid nitrogen, and kept at −80°C until use. GST-CPI and GST-CPI* were purified

by glutathione fast-flow Sepharose resin (GE Healthcare), followed by ion exchange chromatography. His-tagged CPI, CPI*, and CP α1β2 were purified by immobilized metal ion affinity chromatography followed by anion exchange chromatography. NaCl-eluted fractions containing CPI and CP were dialyzed against [20 mM tris (pH 7.8), 40 mM KCl, 0.5 mM DTT, 1 mM EDTA, 20% glycerol] for storage at −80°C. The GBP, His-Avi-GBP, was expressed and biotinylated during isopropyl-β-D-thiogalactopyranoside (IPTG) induction in the BL21* strain transformed with pACYC184-BirA. His-Avi-GBP was purified by Ni-NTA agarose affinity chromatography followed by anion exchange chromatography. NaCl-eluted fractions containing GBP were dialyzed against GBP buffer [20 mM tris (pH 8.0), 100 mM KCl, 2 mM DTT, 1 mM EDTA, 4% glycerol] for storage at −80°C. Purity and protein concentrations were determined after SDS-PAGE using purified actin as a standard, because it is accurately measured by its absorbance at 280 nM. Quantification by densitometry was performed with ImageJ.

Dynactin purification

Native dynactin was purified from pig brains using the previously described large-scale SP Sepharose protocol (*11*). Tagged dynactin was purified from 293 stable cell lines expressing His-mCherry-CPα and Flag-GFP-Arp1 or Flag-GFP-DCTN3. A total of 293 cell pellets were solubilized in buffer [50 mM tris (pH 7.5), 150 mM NaCl, 1% Triton X-100, 4% glycerol, 5 mM $MgSO_4$, 0.1 mM $CaCl_2$, 0.1 mM adenosine 5′-triphosphate (ATP)] supplemented with protease inhibitors. After clarification by centrifugation at 21,000*g* for 40 min, extracts were incubated with equilibrated anti-Flag M2 resin (Sigma-Aldrich). M2 beads were washed in buffer [50 mM tris (pH 7.5), 150 mM NaCl, 0.1% Triton X-100, 0.4% glycerol, 1 mM $MgSO_4$, 0.1 mM $CaCl_2$] and eluted by 3xFlag peptide (150 ng/μl; Sigma-Aldrich) in buffer [35 mM tris (pH 7.5), 150 mM KCl, 0.4 M sucrose, 1 mM $MgCl_2$, 0.1 mM $CaCl_2$, 0.2 mM ATP, 0.1 mM DTT] for 1 hour at 18°C. Eluates were then incubated for 3 hours at 4°C with equilibrated Ni Sepharose High Performance (GE Healthcare). Resin was washed in buffer [35 mM tris (pH 7.5), 150 mM KCl, 0.5 M sucrose, 1 mM $MgCl_2$, 0.1 mM $CaCl_2$, 0.1 mM DTT, 0.2 mM ATP, 5 mM imidazole] and eluted in buffer [35 mM tris (pH 7.5), 150 mM KCl, 0.5 M sucrose, 1 mM $MgCl_2$, 0.1 mM $CaCl_2$, 0.1 mM DTT, 0.2 mM ATP, 150 mM imidazole].

Gel filtration uncapping assays

Dynactin (1.5 μM) was incubated for 5 min at room temperature alone with 3 μM FAM21 CPI, FAM21 CPI*, 15 μM CARMIL1 CPI, or not, in buffer [5 mM tris (pH 7.8), 100 mM KCl, 1 mM $MgCl_2$, 0.1 mM $CaCl_2$, 0.2 mM ATP (pH 7.0), 5 mM DTT]. The mixture was then fractionated on a Superose 6 increase 3.2/300 column on an AKTAmicro system (GE Healthcare). The column was pre-equilibrated and run in the same buffer supplemented with the corresponding CPI.

Negative-stain EM

Dynactin was taken from the peak fraction and diluted 1:3 in buffer [5 mM tris (pH 7.8), 100 mM KCl, 1 mM $MgCl_2$, 0.1 mM $CaCl_2$, 0.2 mM ATP (pH 7.5 to 7.8), 5 mM DTT]. Protein concentrations were chosen to give densely packed particles (approximately 400 per image).

Four hundred mesh copper grids coated with a continuous carbon support layer (Agar Scientific) were treated by glow discharging at 25 mA for 45 s (PELCO EasiGlow). Four microliters of sample was applied to the grid and incubated for 60 s before blotting with filter paper. The grid was then washed in 4× 20-μl 2% uranyl acetate and blotted again before being allowed to dry. Five hundred micrographs per sample were manually collected on a FEI Spirit T12 microscope equipped with Gatan 2K × 2K charge-coupled device (CCD) (model 984). Micrographs were taken with 0.5- to 2.5-μm underfocus at a nominal magnification of 11,000× with a digital pixel size of 4.86 Å.

Micrographs were CTF-corrected using GCTF (*41*). All subsequent processing steps were carried out in RELION-3.0 (*42*). A small set of particles was manually picked and 2D classified, and the filament-like classes were chosen as a template for AutoPicking. Particles were subjected to further 2D classification before 3D classification and 3D refinement using a negative-stain structure of dynactin (*43*) as a reference. The cryo-EM structure of dynactin (Protein Data Bank: 5ADX) (*11*) was fit into the 3D negative-stain maps using UCSF Chimera (*44*).

Actin polymerization assays

Actin was purified from rabbit skeletal muscle acetone powder and kept at 4°C in G buffer [5 mM tris-HCl (pH 7.8), 0.2 mM ATP, 0.1 mM $CaCl_2$, 0.1 mM DTT, 0.01% NaN_3]. Actin was labeled on cysteine-374 with pyrene or labeled on lysines with Alexa 488 or Alexa 568 using standard procedures. The Arp2/3 complex was purchased from Cytoskeleton Inc. Human profilin 1 was expressed and purified in *E. coli* using a polyproline affinity column, and 8 M urea–eluted proteins were dialyzed against profilin storage buffer [10 mM tris-HCl (pH 7.5), 0.1 mM EDTA, 50 mM KCl, 1 mM DTT] and kept at −80°C. Actin and profilin concentrations were determined by absorbance at 280 nm.

Profilin-actin complexes were formed by incubating G-actin with a six- to eightfold molar excess of profilin for 10 min on ice before initiation of polymerization. Dynactin was added to the mix in G buffer. The pyrene actin assay starts upon the addition of one-twentieth volume of 20x KME (2 M KCl, 20 mM $MgCl_2$, 4 mM EGTA). For control curves, an equal amount of buffer without protein was always included. Actin polymerization was monitored by the increase in fluorescence of pyrene-actin (λexc 366 nm, λem 407 nm) at 20°C in a Cary Eclipse spectrofluorimeter (Varian) with a multicell holder. Handling of data and graph drawing were performed using Kaleidagraph v4.03 software (Synergy Software).

Single-filament and single-molecule assays

Open flow chambers were formed by mounting a cleaned glass coverslip on a glass slide with parallel strips of double-sided tape (Fig. 1F). The surface was passivated by incubating a solution of bovine serum albumin (BSA) and biotinylated BSA in the chamber. After rinsing, the chamber was incubated with neutravidin, rinsed, and then incubated with 0.5 μM biotin-labeled GBP in GBP buffer. After rinsing, 2 nM dynactin, or control buffer, was incubated in dynactin buffer [20 mM tris (pH 7.7), 50 mM KCl, 1 mM $MgCl_2$, 0.1 mM $CaCl_2$, 10 mM DTT]. After rinsing, a solution containing 1 μM G-actin (15% Alexa 488–labeled), 8 μM profilin, 30 nM CPI or not, and 0.14% methylcellulose in F-buffer [5 mM tris (pH 7.8), 0.2 mM ATP, 0. 1 mM $CaCl_2$, 10 mM DTT, 1 mM $MgCl_2$, 0.2 mM EGTA, 100 mM KCl, 1 mM 1,4-diazabicyclo[2.2.2]octane] was flowed in and images were acquired in TIRF on an inverted microscope (Nikon TiE, with a 60× TIRF objective) using 100-mW tunable lasers (ILAS2, Gataca Systems), an EMCCD Evolve camera (Photometrics), and MetaMorph software.

The microfluidics experiment (Fig. 1G) was performed in chambers made of polydimethylsiloxane (Sylgard), and solution flows were controlled with a MFCS system (Fluigent) as previously described (*45*). Surfaces were passivated with PEG-Silane (overnight incubation) and then exposed to PLL-PEG-biotin for 1 hour and to PLL-PEG for 10 min and then rinsed extensively. Surfaces were then exposed sequentially to neutravidin, biotin-labeled GBP, and dynactin. Last, a solution containing profilin, Alexa 568–actin (15% labeled), and CPI was flowed in, and images were acquired.

CP-dynactin colocalization experiments (Fig. 2A) were carried out in open flow chambers, passivated with BSA. Solutions of dynactin, preincubated with CPI or CPI* or only buffer, were flowed in, and the chamber was rinsed with buffer after 30 s. For branching experiments (Fig. 3A), preformed filaments of Alexa 568–actin (15% labeled) were mixed with VCA, Arp2/3, and Alexa 488–actin (15% labeled) and flowed into a BSA-passivated chamber.

Isothermal titration calorimetry

CP and CPI proteins were dialyzed against the isothermal titration calorimetry (ITC) buffer [20 mM tris (pH 7.5), 150 mM NaCl, 4% glycerol, and 2 mM β-ME]. Their interaction was analyzed using a MicroCal iTC200 microcalorimeter (GE Healthcare). Measurements were carried out in triplicate at 22°C. GST-CPI, GST-CPI*, or GST at 120 μM was stepwise injected (20 injections of 2 μl every 180 s) from the syringe into the measurement cell containing 9 μM His-tagged CP. No interaction was measured between CP and GST. The change in heating power was observed over the reaction time until equilibrium was reached. Data were analyzed using the software provided by the manufacturer. The graphs show integrated heats of injection with the best fit to a one-site binding model using Origin 7.0 software.

Cell treatments

For transferrin uptake, cells were starved in DMEM supplemented with 0.5% BSA and 10 mM Hepes (pH 7.4) for 30 min and then transferrin (10 μg/ml) coupled with Alexa 555 (Thermo Fisher Scientific) was added for 30 min. Cells were then washed with starvation medium before examination with a confocal microscope.

For 2-NBDG uptake, cells were extensively washed with glucose-free DMEM (Gibco) and then 2-NBDG (100 μg/ml; N13195, Thermo Fisher Scientific) was incubated for 10 min. Cells were then washed with glucose-free DMEM before examination with a confocal microscope.

For the endosomal branched actin regrowth assay, 1 μM latrunculin A (Calbiochem) was incubated for 2 hours, before being extensively washed away.

Recycling assay

Cells in six-well plates were washed with cold phosphate-buffered saline (PBS). Cell surface proteins were labeled with EZ-link cleavable sulfo-NHS-SS-biotin (0.5 mg/ml) (Thermo Fisher Scientific) in Hank's balanced salt solution for 30 min at 4°C. Unbound biotin was washed away with cold medium, and prewarmed serum–containing medium was added to cells. Biotin-labeled surface proteins were allowed to internalize for 30 min at 37°C. The remaining surface-exposed biotin was removed with two washes of reducing buffer (50 mM tris-HCl, 100 mM NaCl, 60 mM MesNa, pH 8.6) for 15 min at 4°C, followed by quenching with (50 mM tris-HCl, 100 mM NaCl, 100 mM iodoacetamide, pH 8.0) for 15 min on ice. The cells were incubated at 37°C for 0, 15, 30, and 60 min and then exposed to reduction and quenching as above. Cells were washed with cold PBS and lysed by scraping in 100 μl of lysis buffer [50 mM tris-HCl, 150 mM NaCl, 1.5% octylglucoside, 1% NP-40, 1 mM EDTA (pH 7.4) supplemented with protease inhibitors] and incubated at 4°C for 20 min. Cell extracts were cleared by centrifugation (16,000*g*, 20 min, 4°C). After bicinchoninic acid normalization, samples were incubated for 3 hours with streptavidin beads (Thermo Fisher Scientific), washed five times, and analyzed by Western blot.

Immunofluorescence

Cells were fixed either in 3.2% paraformaldehyde (PFA) prepared in PBS or in 1% PFA in serum-free DMEM followed by absolute methanol at −20°C in the case of GLUT1 staining. Cells were quenched with 50 mM NH_4Cl, then permeabilized with 0.5% Triton X-100, blocked in 2% BSA, and incubated with antibodies (1 to 5 μg/ml for the primary, 5 μg/ml for the secondary). Images were acquired using a Leica SP8ST-WS confocal microscope equipped with an HC PL APO 63×/1.40 oil immersion objective, a white light laser, HyD, and photomultiplier tube detectors.

Live fast acquisition microscopy

Live cells were plated on fibronectin-coated glass-bottom petri dishes (World Precision Instruments) for 2 hours at 37°C and imaged in Leibovitz's L-15 Medium without phenol red (Thermo Fisher Scientific) on a custom spinning disk confocal microscope composed of a Nikon Ti stand equipped with perfect focus, a 100× numerical aperture (NA) 1.49 SR TIRF objective, a Yokogawa CSU-X1 spinning disk head, and a Photometrics 95B back-illuminated sCMOS (scientific complementary metal–oxide–semiconductor) camera operating in global shutter mode. Excitation was performed using 488-nm (150 mW OBIS LX), 561-nm (100 mW OBIS LS), and 637-nm (140 mW OBIS LX) lasers fibered by a Cairn laser launch. To minimize bleed through, single-band emission filters were used (Chroma 525/50 for GFP, 595/50 for mCherry, and 680/40 for iRFP) and acquisition of each channel was performed sequentially using a fast filter wheel (Cairn Optospin). Sample temperature was maintained at 37°C using a temperature control chamber (Digital Pixel Microscopy System). Acquisition was controlled by MetaMorph software.

For the TIRF imaging, cells were spread overnight on fibronectin-coated glass (20 μg/ml in PBS for 1 hour for the coating) and imaged in Leibovitz's L-15 medium (Gibco) supplemented with 20 mM Hepes (Gibco) at 37°C using a temperature control chamber (Digital Pixel Microscopy System). TIRF imaging was performed on a custom-built TIRF system based a Nikon Ti stand equipped with perfect focus system, a fast Z piezo stage (ASI), a PLAN NA 1.45 100× objective, and an azimuthal TIRF illuminator (iLas2, Roper France) modified to have an extended field of view (Cairn). Images were recorded with a Photometrics Prime 95B back-illuminated sCMOS camera run in pseudo-global shutter mode and synchronized with the azimuthal illumination. GFP (respectively mCherry and iRFP670) was excited by a 488-nm laser (respectively 561 and 637 nm, all Coherent OBIS mounted in a Cairn laser launch) and imaged using dedicated single band-pass filters for each channel mounted on a Cairn Optospin wheel (Chroma 525/50 for GFP and Chroma 595/50 for mCherry and 655LP for iRFP). TIRF angle was set independently for all channels so that the depth of the TIRF field was identical for all channels. The system was operated by MetaMorph.

To enhance the detection of dim endosomes in live imaging data (Fig. 3B, fig. S7, and movie S2), a wavelet "à trous" filter (*9*) was

applied to raw images and the resulting filtered image was averaged with the original raw image. This treatment was not applied when colocalization was quantified. Endosome trajectories were used as the lines for kymograph measurement.

Videomicroscopy of cell migration

Videomicroscopy was performed on an inverted Axio Observer microscope (Zeiss) equipped with a Pecon Zeiss incubator XL multi S1 RED LS (Heating Unit XL S, Temp module, CO2 module, Heating Insert PS, and CO2 cover), a definite focus module, and a Hamamatsu camera (C10600 Orca-R2). Pictures were taken every 5 min for 24 hours using the Plan-Apochromat 20×/0.80 air objective. In the single cell migration assay, only the cells that were freely migrating for 12 hours were taken into account. Cell trajectories were acquired with the ImageJ Manual tracking plugin. Analysis of cell migration was performed in the DiPer software (*46*). To measure aspect ratio, the ratio of the longest axis of a cell to the shortest one, cell boundaries were manually drawn. Volatility corresponds to its SD at all time points.

Image analysis

Image analysis was performed in ImageJ or FIJI software. To measure endosomal enrichment of ARPC2 staining, images were thresholded in the VPS35 channel by the Otsu algorithm to create a region of interest (ROI) and then the mean intensity of the ARPC2 staining was measured in this ROI. Endosomal enrichment was defined as the ratio of mean ARPC2 intensity in the ROI divided by the mean intensity of ARPC2 in the whole cell. Similarly, perinuclear enrichment of GLUT1 was defined as the ratio of GLUT1 intensity in a disc of 100 μm^2 that contains most of the GLUT1 signal in the perinuclear region divided by the one of the whole cell. Mean fluorescent intensities of 2-NBDG in the nucleus and in the whole cell were quantified. Cytoplasmic accumulation is defined as the difference between total and nuclear intensity.

To automatically measure colocalization between mCherry-DCTN6, GFP-ARPC5, and iRFP670-WASH, we used an object-based method, where two objects are considered delocalized if the distance between their fluorescence centroid (d) is below a certain threshold d_{ref}, usually set close to lateral resolution of the microscope (r_{xy}) (*47*). To segment endosomes, we used a threshold-free method based on 2D Gaussian fitting, which does not rely on an intensity threshold, but rather on the fact that particles have a Gaussian shape against the local background [Thunderstorm algorithm (*48*)]. Once this automated segmentation has been performed in all three channels, the distance d between all objects in the iRFP670-WASH and mCherry-DCTN6 (respectively GFP-ARPC5) channels is computed and compared to the distance threshold (d_{ref} = 0.36 μm; measured using 0.2-μm TetraSpeck beads from Invitrogen). Once all the particles have been detected and their colocalization state has been addressed (i.e., $d < d_{ref}$), we measured the percentage of colocalization. This measurement was averaged over five time points to avoid false-positive colocalization events because of particles detected in both channels at the same time by chance and then this was averaged between cells.

Statistics

Statistical analysis was carried out with GraphPad Prism software (v7.00) and Microsoft Excel 2016. When not stated otherwise, analysis of variance (ANOVA) and Kruskal-Wallis test were used for the statistical analysis. Shapiro-Wilk normality test was applied to examine whether data samples fit a normal distribution. If data satisfied the normality criterion, then ANOVA followed by post hoc Tukey's multiple comparison test was performed. If not, then nonparametric Kruskal-Wallis test followed by post hoc Dunn's multiple comparison test was applied. Four levels of significance were distinguished: $*P < 0.05$, $**P < 0.01$, $***P < 0.001$, $****P < 0.0001$. n refers to the number of independent experiments.

SUPPLEMENTARY MATERIALS

Supplementary material for this article is available at http://advances.sciencemag.org/cgi/content/full/7/3/eabd5956/DC1

REFERENCES AND NOTES

1. O. Alekhina, E. Burstein, D. D. Billadeau, Cellular functions of WASP family proteins at a glance. *J. Cell Sci.* **130**, 2235–2241 (2017).
2. E. Derivery, C. Sousa, J. J. Gautier, B. Lombard, D. Loew, A. Gautreau, The Arp2/3 activator WASH controls the fission of endosomes through a large multiprotein complex. *Dev. Cell* **17**, 712–723 (2009).
3. T. S. Gomez, D. D. Billadeau, A FAM21-containing WASH complex regulates retromer-dependent sorting. *Dev. Cell* **17**, 699–711 (2009).
4. D. Jia, T. S. Gomez, Z. Metlagel, J. Umetani, Z. Owitnowski, M. K. Rosen, D. D. Billadeau, WASH and WAVE actin regulators of the Wiskott–Aldrich syndrome protein (WASP) family are controlled by analogous structurally related complexes. *Proc. Natl. Acad. Sci. U.S.A.* **107**, 10442–10447 (2010).
5. M. Edwards, A. Zwolak, D. A. Schafer, D. Sept, R. Dominguez, J. A. Cooper, Capping protein regulators fine-tune actin assembly dynamics. *Nat. Rev. Mol. Cell Biol.* **15**, 677–689 (2014).
6. M. Hernandez-Valladares, T. Kim, B. Kannan, A. Tung, A. H. Aguda, M. Larsson, J. A. Cooper, R. C. Robinson, Structural characterization of a capping protein interaction motif defines a family of actin filament regulators. *Nat. Struct. Mol. Biol.* **17**, 497–503 (2010).
7. S. Takeda, S. Minakata, R. Koike, I. Kawahata, A. Narita, M. Kitazawa, M. Ota, T. Yamakuni, Y. Maéda, Y. Nitanai, Two distinct mechanisms for actin capping protein regulation—Steric and allosteric inhibition. *PLOS Biol.* **8**, e1000416 (2010).
8. M. Edwards, P. McConnell, D. A. Schafer, J. A. Cooper, CPI motif interaction is necessary for capping protein function in cells. *Nat. Commun.* **6**, 8415 (2015).
9. E. Derivery, E. Helfer, V. Henriot, A. Gautreau, Actin polymerization controls the organization of WASH domains at the surface of endosomes. *PLOS ONE* **7**, e39774 (2012).
10. T. A. Schroer, Dynactin. *Annu. Rev. Cell Dev. Biol.* **20**, 759–779 (2004).
11. L. Urnavicius, K. Zhang, A. G. Diamant, C. Motz, M. A. Schlager, M. Yu, N. A. Patel, C. V. Robinson, A. P. Carter, The structure of the dynactin complex and its interaction with dynein. *Science* **347**, 1441–1446 (2015).
12. M. E. Harbour, S. Y. Breusegem, M. N. J. Seaman, Recruitment of the endosomal WASH complex is mediated by the extended "tail" of Fam21 binding to the retromer protein Vps35. *Biochem. J.* **442**, 209–220 (2012).
13. D. Jia, T. S. Gomez, D. D. Billadeau, M. K. Rosen, Multiple repeat elements within the FAM21 tail link the WASH actin regulatory complex to the retromer. *Mol. Biol. Cell* **23**, 2352–2361 (2012).
14. E. Helfer, M. E. Harbour, V. Henriot, G. Lakisic, C. Sousa-Blin, L. Volceanov, M. N. J. Seaman, A. Gautreau, Endosomal recruitment of the WASH complex: Active sequences and mutations impairing interaction with the retromer. *Biol. Cell* **105**, 191–207 (2013).
15. T. Wassmer, N. Attar, M. Harterink, J. R. T. van Weering, C. J. Traer, J. Oakley, B. Goud, D. J. Stephens, P. Verkade, H. C. Korswagen, P. J. Cullen, The retromer coat complex coordinates endosomal sorting and dynein-mediated transport, with carrier recognition by the trans-Golgi network. *Dev. Cell* **17**, 110–122 (2009).
16. M. N. J. Seaman, Retromer and its role in regulating signaling at endosomes. *Prog. Mol. Subcell. Biol.* **57**, 137–149 (2018).
17. J. L. Ross, K. Wallace, H. Shuman, Y. E. Goldman, E. L. F. Holzbaur, Processive bidirectional motion of dynein-dynactin complexes in vitro. *Nat. Cell Biol.* **8**, 562–570 (2006).
18. T. D. Pollard, J. A. Cooper, Quantitative analysis of the effect of Acanthamoeba profilin on actin filament nucleation and elongation. *Biochemistry* **23**, 6631–6641 (1984).
19. T. D. Pollard, Regulation of actin filament assembly by Arp2/3 complex and formins. *Annu. Rev. Biophys. Biomol. Struct.* **36**, 451–477 (2007).
20. V. Achard, J.-L. Martiel, A. Michelot, C. Guérin, A.-C. Reymann, L. Blanchoin, R. Boujemaa-Paterski, A "primer"-based mechanism underlies branched actin filament network formation and motility. *Curr. Biol.* **20**, 423–428 (2010).
21. T.-Y. Yeh, N. J. Quintyne, B. R. Scipioni, D. M. Eckley, T. A. Schroer, Dynactin's pointed-end complex is a cargo-targeting module. *Mol. Biol. Cell* **23**, 3827–3837 (2012).

22. M. J. Taylor, D. Perrais, C. J. Merrifield, A high precision survey of the molecular dynamics of mammalian clathrin-mediated endocytosis. *PLOS Biol.* **9**, e1000604 (2011).
23. M. A. Puthenveedu, B. Lauffer, P. Temkin, R. Vistein, P. Carlton, K. Thorn, J. Taunton, O. D. Weiner, R. G. Parton, M. von Zastrow, Sequence-dependent sorting of recycling proteins by actin-stabilized endosomal microdomains. *Cell* **143**, 761–773 (2010).
24. A. Gautreau, K. Oguievetskaia, C. Ungermann, Function and regulation of the endosomal fusion and fission machineries. *Cold Spring Harb. Perspect. Biol.* **6**, a016832 (2014).
25. T. Zech, S. D. J. Calaminus, P. Caswell, H. J. Spence, M. Carnell, R. H. Insall, J. Norman, L. M. Machesky, The Arp2/3 activator WASH regulates α5β1-integrin-mediated invasive migration. *J. Cell Sci.* **124**, 3753–3759 (2011).
26. S. N. Duleh, M. D. Welch, Regulation of integrin trafficking, cell adhesion, and cell migration by WASH and the Arp2/3 complex. *Cytoskeleton* **69**, 1047–1058 (2012).
27. F. Steinberg, M. Gallon, M. Winfield, E. C. Thomas, A. J. Bell, K. J. Heesom, J. M. Tavaré, P. J. Cullen, A global analysis of SNX27-retromer assembly and cargo specificity reveals a function in glucose and metal ion transport. *Nat. Cell Biol.* **15**, 461–471 (2013).
28. J. T. Piotrowski, T. S. Gomez, R. A. Schoon, A. K. Mangalam, D. D. Billadeau, WASH knockout T cells demonstrate defective receptor trafficking, proliferation, and effector function. *Mol. Cell. Biol.* **33**, 958–973 (2013).
29. Y. Liang, H. Niederstrasser, M. Edwards, C. E. Jackson, J. A. Cooper, Distinct roles for CARMIL isoforms in cell migration. *Mol. Biol. Cell* **20**, 5290–5305 (2009).
30. M. Edwards, Y. Liang, T. Kim, J. A. Cooper, Physiological role of the interaction between CARMIL1 and capping protein. *Mol. Biol. Cell* **24**, 3047–3055 (2013).
31. P. Soubeyran, K. Kowanetz, I. Szymkiewicz, W. Y. Langdon, I. Dikic, Cbl-CIN85-endophilin complex mediates ligand-induced downregulation of EGF receptors. *Nature* **416**, 183–187 (2002).
32. A. Petrelli, G. F. Gilestro, S. Lanzardo, P. M. Comoglio, N. Migone, S. Giordano, The endophilin-CIN85-Cbl complex mediates ligand-dependent downregulation of c-Met. *Nature* **416**, 187–190 (2002).
33. L. Urnavicius, C. K. Lau, M. M. Elshenawy, E. Morales-Rios, C. Motz, A. Yildiz, A. P. Carter, Cryo-EM shows how dynactin recruits two dyneins for faster movement. *Nature* **554**, 202–206 (2018).
34. H. L. Sladitschek, P. A. Neveu, MXS-Chaining: A highly efficient cloning platform for imaging and flow cytometry approaches in mammalian systems. *PLOS ONE* **10**, e0124958 (2015).
35. T. H. Millard, B. Behrendt, S. Launay, K. Fütterer, L. M. Machesky, Identification and characterisation of a novel human isoform of Arp2/3 complex subunit p16-ARC/ARPC5. *Cell Motil. Cytoskeleton* **54**, 81–90 (2003).
36. N. Molinie, S. N. Rubtsova, A. Fokin, S. P. Visweshwaran, N. Rocques, A. Polesskaya, A. Schnitzler, S. Vacher, E. V. Denisov, L. A. Tashireva, V. M. Perelmuter, N. V. Cherdyntseva, I. Bièche, A. M. Gautreau, Cortical branched actin determines cell cycle progression. *Cell Res.* **29**, 432–445 (2019).
37. U. Rothbauer, K. Zolgadr, S. Muyldermans, A. Schepers, M. C. Cardoso, H. Leonhardt, A versatile nanotrap for biochemical and functional studies with fluorescent fusion proteins. *Mol. Cell. Proteomics* **7**, 282–289 (2008).
38. F. González, Z. Zhu, Z.-D. Shi, K. Lelli, N. Verma, Q. V. Li, D. Huangfu, An iCRISPR platform for rapid, multiplexable, and inducible genome editing in human pluripotent stem cells. *Cell Stem Cell* **15**, 215–226 (2014).
39. E. Derivery, A. Gautreau, Assaying WAVE and WASH complex constitutive activities toward the Arp2/3 complex. *Methods Enzymol.* **484**, 677–695 (2010).
40. S. P. Visweshwaran, P. A. Thomason, R. Guerois, S. Vacher, E. V. Denisov, L. A. Tashireva, M. E. Lomakina, C. Lazennec-Schurdevin, G. Lakisic, S. Lilla, N. Molinie, V. Henriot, Y. Mechulam, A. Y. Alexandrova, N. V. Cherdyntseva, I. Bièche, E. Schmitt, R. H. Insall, A. Gautreau, The trimeric coiled-coil HSBP1 protein promotes WASH complex assembly at centrosomes. *EMBO J.* **37**, e97706 (2018).
41. K. Zhang, Gctf: Real-time CTF determination and correction. *J. Struct. Biol.* **193**, 1–12 (2016).
42. J. Zivanov, T. Nakane, B. O. Forsberg, D. Kimanius, W. J. H. Hagen, E. Lindahl, S. H. W. Scheres, New tools for automated high-resolution cryo-EM structure determination in RELION-3. *eLife* **7**, e42166 (2018).
43. S. Chowdhury, S. A. Ketcham, T. A. Schroer, G. C. Lander, Structural organization of the dynein–dynactin complex bound to microtubules. *Nat. Struct. Mol. Biol.* **22**, 345–347 (2015).
44. E. F. Pettersen, T. D. Goddard, C. C. Huang, G. S. Couch, D. M. Greenblatt, E. C. Meng, T. E. Ferrin, UCSF Chimera—A visualization system for exploratory research and analysis. *J. Comput. Chem.* **25**, 1605–1612 (2004).
45. A. Jégou, T. Niedermeyer, J. Orban, D. Didry, R. Lipowsky, M.-F. Carlier, G. Romet-Lemonne, Individual actin filaments in a microfluidic flow reveal the mechanism of ATP hydrolysis and give insight into the properties of profilin. *PLOS Biol.* **9**, e1001161 (2011).
46. R. Gorelik, A. Gautreau, Quantitative and unbiased analysis of directional persistence in cell migration. *Nat. Protoc.* **9**, 1931–1943 (2014).
47. S. Bolte, F. P. Cordelières, A guided tour into subcellular colocalization analysis in light microscopy. *J. Microsc.* **224**, 213–232 (2006).
48. M. Ovesný, P. Křížek, J. Borkovec, Z. Svindrych, G. M. Hagen, ThunderSTORM: A comprehensive ImageJ plug-in for PALM and STORM data analysis and super-resolution imaging. *Bioinformatics* **30**, 2389–2390 (2014).
49. L. Cao, M. Kerleau, E. L. Suzuki, H. Wioland, S. Jouet, B. Guichard, M. Lenz, G. Romet-Lemonne, A. Jegou, Modulation of formin processivity by profilin and mechanical tension. *eLife* **7**, e34176 (2018).
50. R. Dominguez, K. C. Holmes, Actin structure and function. *Annu. Rev. Biophys.* **40**, 169–186 (2011).
51. K. A. Melkonian, K. C. Maier, J. E. Godfrey, M. Rodgers, T. A. Schroer, Mechanism of dynamitin-mediated disruption of dynactin. *J. Biol. Chem.* **282**, 19355–19364 (2007).

Acknowledgments: We thank P. Lappalainen and D. Billadeau for gifts of DNA constructs, L. Blanchoin for the gift of profilin, P. Mahou for assistance in confocal microscopy, and J. Boulanger for image processing advice. **Funding:** This work was supported in A.M.G.'s group by grants from the Agence Nationale de la Recherche (ANR ANR-15-CE13-0016-01), from the Fondation ARC pour la Recherche sur le Cancer (PGA120140200831), and from Institut National du Cancer (INCA_6521). E.D. is supported by the Medical Research Council (MC_UP_1201/13) and the Human Frontier Science Program (CDA00034/2017). The imaging facility of Laboratoire d'Optique et Biosciences (Ecole Polytechnique) is partly supported by Agence Nationale de la Recherche (ANR-11-EQPX-0029 Morphoscope2). **Author contributions:** A.I.F. established most stable cell lines, characterized them, and performed all cell biology experiments. V.D. purified most recombinant proteins and performed pyrene actin assays. C.L.C. supervised some actin polymerization assays. N.R. purified some recombinant proteins and the dually tagged dynactin by tandem affinity purification. L.C. and G.R.-L. performed in vitro TIRF assays. G.R.-L. supervised all of them. C.E.S. purified pig brain dynactin and performed gel filtration analysis. C.E.S. and A.P.C. performed EM reconstruction of uncapped dynactin. M.A.-N. performed ITC measurements. K.O. cloned dynactin subunits and created the animated model. K.O. and M.-V.H. performed coimmunoprecipitation in brain extracts under the supervision of F.S. E.D. performed live confocal microscopy. V.H. prepared several DNA constructs. N.M. constructed an expression vector and derived the corresponding stable cell line. A.I.F. drafted the manuscript. A.M.G. supervised the work and wrote the manuscript. A.I.F. and V.D. contributed to the conceptual development of the project. **Competing interests:** The authors declare that they have no competing interests. **Data and materials availability:** Data needed to evaluate the conclusions in the paper are present in the paper or the Supplementary Materials. All data and the custom code to assess the three-color colocalization are available from the authors upon reasonable request.

Submitted 30 June 2020
Accepted 18 November 2020
Published 13 January 2021
10.1126/sciadv.abd5956

Citation: A. I. Fokin, V. David, K. Oguievetskaia, E. Derivery, C. E. Stone, L. Cao, N. Rocques, N. Molinie, V. Henriot, M. Aumont-Nicaise, M.-V. Hinckelmann, F. Saudou, C. Le Clainche, A. P. Carter, G. Romet-Lemonne, A. M. Gautreau, The Arp1/11 minifilament of dynactin primes the endosomal Arp2/3 complex. *Sci. Adv.* **7**, eabd5956 (2021).

The Arp1/11 minifilament of dynactin primes the endosomal Arp2/3 complex

Artem I. Fokin, Violaine David, Ksenia Oguievetskaia, Emmanuel Derivery, Caroline E. Stone, Luyan Cao, Nathalie Rocques, Nicolas Molinie, Véronique Henriot, Magali Aumont-Nicaise, Maria-Victoria Hinckelmann, Frédéric Saudou, Christophe Le Clainche, Andrew P. Carter, Guillaume Romet-Lemonne and Alexis M. Gautreau

Sci Adv **7** (3), eabd5956.
DOI: 10.1126/sciadv.abd5956